ACS OMEGA

Article

Cite This: ACS Omega 2019, 4, 17090−17097

http://pubs.acs.org/journal/acsodf

Covalently Fluorophore-Functionalized ZIF-8 Colloidal Particles as a Sensing Platform for Endocrine-Disrupting Chemicals Such as Phthalates Plasticizers

Ander Chapartegui-Arias,[†,‡] Jose A. Villajos,[†] Anett Myxa,[†] Sebastian Beyer,[†,§] Jana Falkenhagen,[†] Rudolf J. Schneider,[†,∥] and Franziska Emmerling*[,†]

[†]Federal Institute for Materials Research and Testing (BAM), Richard-Willstätter-Straße 11, D-12489 Berlin, Germany

[‡]Department of Chemistry, Humboldt-Universität zu Berlin, Brook-Taylor-Straße 2, D-12489 Berlin, Germany

[§]Department of Biomedical Engineering, Chinese University of Hong Kong, Room 802, 8/F, William M.W. Mong Engineering Building, Sha Tin, Hong Kong Special Administrative Region (SAR), China

[∥]Technische Universität Berlin, Straße des 17. Juni 135, D-10623 Berlin, Germany

Supporting Information

ABSTRACT: We present the optical sensing of phthalate esters (PAEs), a group of endocrine-disrupting chemicals. The sensing takes place as changes in the fluorescence emission intensity of aminopyrene covalently bound to the organic ligands of the metal−organic framework compound ZIF-8. In the presence of PAEs, a quenching of the fluorescence emission is observed. We evaluated strategies to engineer colloidal size distribution of the sensing particles to optimize the sensory response to PAEs. A thorough characterization of the modified ZIF-8 nanoparticles included powder X-ray diffractometry, transmission electron microscopy, high-performance liquid chromatography, and photophysical characterization. The presented capability of the fluorophore-functionalized ZIF-8 to sense PAEs complements established methods such as chromatography-based procedures, which cannot be used on-site and paves the way for future developments such as hand-held quick sensing devices.

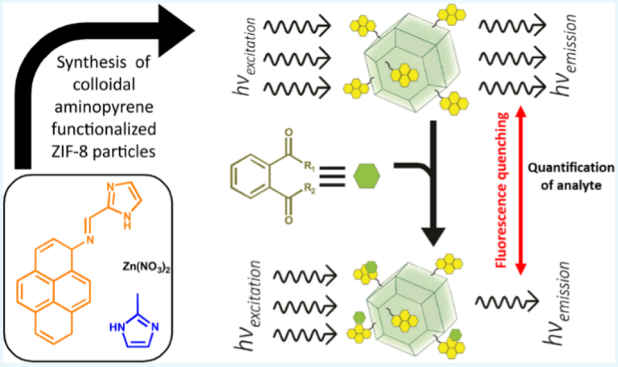

INTRODUCTION

Endocrine-disrupting chemicals are substances that disturb the hormonal balance in complex biological life forms.[1] Increased levels of phthalates are associated with severe consequences in the developmental biology of children, decreased fertility, increased risk of diabetes, and increased malignancy of cancer in adults.[2] In this context, the development of new sensor systems for phthalates is of interest since phthalates are widely used in consumer products. Applications include the use as plasticizers in plastic-made tableware for children, toys, drinking bottles, and other poly(vinyl chloride)-based products (e.g., floor cover material),[3] to name a few.

Currently, the predominantly used methodology to test for the presence of phthalates in a given sample requires advanced analytical methods, for example, techniques such as liquid chromatography coupled to mass spectrometry.[4] This technology is immobile, restricting the routine on-site monitoring of the presence of phthalates to ensure consumer safety. The availability of a reusable sensor capable of measuring on-site without the requirement of specialized personnel implies a big advantage for safety and quality control and would have a considerable economic impact. When developing a new sensing system, the approach of using a sensor compound dissolved in the sample implies that the sensor will not be easily recoverable; therefore, the sensor cannot be reused unless costly separation/regeneration processes are carried out. Thus, a potentially expensive product is lost and disposing of the waste may increase costs. The heterogenization of the chromophore bound to a solid surface offers a big advantage over direct use of the chromophore in solution, making it easier to recover from a suspension for its reuse. It also offers a higher number of possibilities to adapt its use as a sensing device.

Short-chained phthalates are basically nonpolar substances, with their hydrophobicity increasing with chain length. Poor solubility in water limits their analysis in typical quick sensing technologies and especially the development of antibodies needed for immunoanalytical techniques. While specific antibodies, as a basis for such formats, could be generated for short-chained phthalates [dibutylphthalate (DBP)[5−7] and

Received: April 12, 2019
Accepted: August 22, 2019
Published: October 10, 2019

DOI: 10.1021/acsomega.9b01051
ACS Omega 2019, 4, 17090−17097

dimethylphthalate (DMP[8])], it was not the case for the much more important, long-chained phthalates [diethylhexylphthalate (DEHP) and benzylbutylphthalate (BBP)] or their substitutes, such as diisononyl 1,2-cyclohexanedicarboxylic acid.[9]

In this context, the use of zeolitic imidazolate frameworks (ZIFs), a subclass of metal−organic frameworks (MOFs), might offer an analytical approach as a support for the sensor moiety. These MOFs are attractive due to their regular pore size, high porosity, excellent mechanical stability, tunable surface properties, and their exceptional chemical and thermal stabilities.[10,11] The combination of these features distinguishes ZIFs from many other MOFs. ZIFs are exceptionally easy to synthesize through precipitation reactions from aqueous and organic solvents.[12] Structurally, ZIFs are grown from imidazolate tetrahedra constructed by the coordination between metallic cations and imidazolate anions,[10,13] where imidazole and imidazole derivative units constitute the bridges for connecting the metal centers. The pore size and the adsorption properties of ZIFs can be tailored by changing or chemically modifying the anionic imidazolate linker.[14] The intrinsic properties of ZIFs have led to their use in a broad range of applications including sensing,[15] catalysis,[16] and extraction,[17] to name a few. In addition, the known hydrophobicity of some of these ZIF materials[18] makes them suitable for analyzing the nonpolar phthalates in aqueous solution, preconcentrating these analytes, thus potentially increasing sensitivity. This effect has been reported for other MOFs, like MIL-101[19] being used for the adsorptive removal of polypropylene co-polymers.

Among ZIFs, the ZIF-8 is advantageous due to its properties, especially its high porosity, high hydrothermal stability, and hydrophobicity. Moreover, their synthesis is inexpensive, straightforward, and reproducible and they are even commercially available. Using ZIF-8 as a sensor scaffold requires to bind fluorescent pyrene derivatives to its backbone. Pyrene is known for its ability to form excimers with aromatic components. The high quantum yield and long fluorescence lifetime make it an ideal candidate for sensing of aromatic molecules, which can be seen in some examples such as the work by Rochat et al. that uses sulfonated water-soluble pyrene derivatives to detect caffeine in aqueous samples.[20] We decided to adapt this approach as a sensing principle for PAEs, by including an aminopyrene core in the structure of ZIF-8. The modification for the structure of ZIF-8 was carried out by combining two methodologies: (i) we include an imidazole derivative on the ZIF-8 structure with a carboxaldehyde functionality, which allowed to covalently bind the pyrene core on the ZIF-8 structure via imine formation condensation and (ii) we applied a reported methodology to obtain ZIF-8 nanoparticles by adding *N*-butylamine as a modulating agent during the synthesis process.[21] By combining these processes, we obtained a nanoparticulated solid MOF capable of performing sensing against dissolved aromatic analytes of high interest, such as PAEs.

RESULTS AND DISCUSSION

Synthetic Route of Z8P-0.25 to Z8P-5.00 MOFs. To include the pursued functionalization on the structure of ZIF-8, the original synthesis[11] had to be modified. We used two reported modifications for the standard ZIF-8 synthesis: (i) the inclusion of 1-metylimidazole and *n*-butylamine as modulating agents[21] during the formation of the ZIF to obtain a nanoparticulate MOF and (ii) the inclusion of the fluorescent chromophore on the structure, via Schiff's base condensation between 2-imidazolecarboxaldehyde and 1-aminopyrene.

For this second modification, we adapted the methodology reported by Yaghi et al.,[22] in which they functionalize the organic linkers of ZIF-90 (2-imidazolecarboxaldehyde) post-synthetically using mild organic reactions, forming ZIF-92. However, in our system the condensation between 2-imidazolecarboxaldehyde and 1-aminopyrene had to be done prior to the formation of the ZIF. The modulating agent agent *n*-butylamine, key for the formation of colloidal particles of ZIF-8, has an even higher affinity for Schiff's base condensation, which leads to a blocking of the 2-imidazolecarboxaldehyde positions and prevents the covalent incorporation of 1-aminopyrene into the modified ZIF-8 framework. Thus, the condensation between 2-imidazolecarboxaldehyde and 1-aminopyrene had to be done prior to the formation of the ZIF. After this first reaction, the formation of the ZIF proceeds, resulting in a nanosized, modified ZIF-8 structure. The powder X-ray diffraction patterns of the modified ZIF-8 (Z8P) is similar to that of the unmodified ZIF-8 (Figures 1 and S1a−e; Supporting Information).

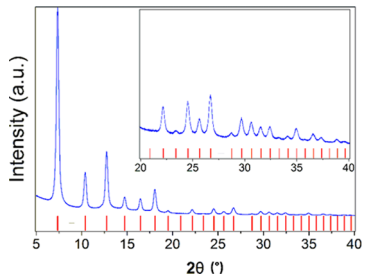

Figure 1. Measured powder diffraction pattern for Z8P-5.00 (blue line) compared to the reflection positions of that of the unmodified ZIF-8 (red bars).

Transmission electron microscopy (TEM) images show that the nanoparticles have sizes between 20 and 50 nm in diameter (Supporting Information, Figure S2a−d). The particle size is relevant since it is a key factor for the reproducibility of the fluorescence measurements, assuming there are two areas of the particle where the quenching can happen: (i) on the surface of the particle and (ii) on the inside of the particles. We hypothesize that each zone causes quenching by different mechanisms,[23] which had to be proven by the characterization of fluorescence properties. Another relevant reason for obtaining nanoparticles is the homogeneity of the resulting suspensions that are stable without further surface modifications that would otherwise be required.[24]

Composition of Z8P MOFs via High-performance Liquid Chromatography (HPLC). To determine the exact proportion of the imidazole components on the different Z8P-0.25 to Z8P-5 MOFs, high-performance liquid chromatography (HPLC) was used. An applicable methodology has been reported by Bennett et al.,[25] where HPLC was used to quantify the final composition of ZIF-62.

To quantify the composition of MOFs Z8P-0.25 to Z8P-5.00, they had to be digested first. For this purpose, 10 mg of each of the ZIFs was suspended in 5 mL of the HPLC eluent and 100 μL of aqueous 1 M solution of HCl was added. The suspended particles slowly dissolved, forming a clear yellow solution. This solution was injected into the HPLC system.

DOI: 10.1021/acsomega.9b01051
ACS Omega 2019, 4, 17090−17097

Retention times of the starting materials of Z8P-0.25 to Z8P-5.00 MOFs were recorded (Supporting Information, Figure S3a). Each species showed a single peak that can be distinguished from the others, except for Z8P-S (the product of the Schiff base conjugation between 2-imidazolcarboxaldehyde and 1-aminopyrene, Supporting Information, Figure S3b), which showed two peaks corresponding to 1-aminopyrene and 2-imidazolecarboxaldehyde. Further studies by mass spectrometry (Supporting Information, Figure S3c) proved that Z8P-S decomposes on aqueous acidic conditions[26] into its chemical constituents. For further quantification of Z8P-S on the different Z8P MOFs, the 1-aminopyrene signal was used since both constituents have 1:1 stoichiometry on the resulting modified ZIF.

During the quantification process for the constituents of Z8P MOFs, we realized that no 1-methylimidazole was present (Figure 2, top). This ligand was expected to act as a

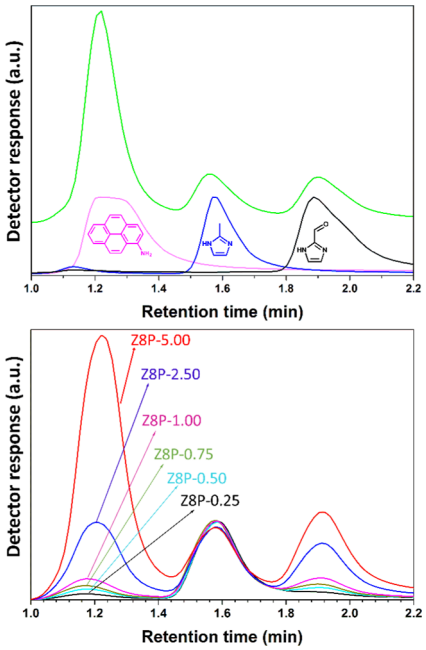

Figure 2. Top: chromatogram for the digested Z8P-5.00 together with the chromatograms for 1-aminopyrene, 2-methylinidazolecarboxaldehyde, and 2-methylimidazole. Bottom: chromatograms of the different variants of Z8P.

competitive ligand in the coordination sphere of zinc,[21] thus being part of the modified ZIF structure. However, its absence after digestion suggests that the ligand acts only as a modulating agent during the synthesis of Z8P MOFs.

Table 1 summarizes initial and measured molar proportions (in mole percent) for each of the components of the different Z8P MOFs. Results show that an increase in the initial concentration of the constituents leads to an increase in the concentration of 1-aminopyrene and imidazolecarboxaldehyde, allowing to tune the maximum intensity of the fluorescence emission. This conjugation, however, is not linear (Supporting Information, Figure S3f), yet it was still possible to predict the final amount of fluorophore on the Z8P MOF, tuning its maximum fluorescence emission and allowing to synthesize the modified ZIF with the ideal fluorescence intensity to mass ratio.

Table 1. Initial and Measured Molar Proportions (in Percent) for Each of the Components for Z8P MOFs

	2-AmiPyr	2-ImiCarb	2-MeImi	1-MeImi
initial proportions (mol %)				
Z8P-0.25	0.250	0.250	49.750	49.750
Z8P-0.50	0.500	0.500	49.500	49.500
Z8P-0.75	0.750	0.750	49.250	49.250
Z8P-1.00	1.000	1.000	49.000	49.000
Z8P-2.50	2.500	2.500	47.500	47.500
Z8P-5.00	5.000	5.000	45.000	45.000
measured proportions (mol %)				
Z8P-0.25	0.058	5.530	94.412	0.000
Z8P-0.50	0.099	6.941	92.961	0.000
Z8P-0.75	0.126	7.953	91.921	0.000
Z8P-1.00	0.183	9.746	90.070	0.000
Z8P-2.50	0.613	20.111	79.276	0.000
Z8P-5.00	1.635	27.305	71.060	0.000

Porosity Characterization of Z8P-5.00. Figure 3 shows the adsorption−desorption isotherms for N_2 at −196 °C for

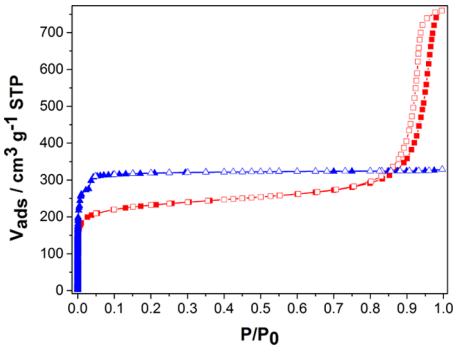

Figure 3. N_2 adsorption−desorption isotherms at −196 °C for materials ZIF-8 NP (blue triangles) and Z8P-5.00 (red squares). Solid and open symbols correspond to adsorption and desorption branches, respectively.

Z8P-5.00 and, for comparison, the nanoparticulate ZIF-8 (ZIF-8 NP). ZIF-8 shows a type I isotherm corresponding to microporous materials according to the International Union of Pure and Applied Chemistry classification.[27] Z8P-5.00 shows a type IV isotherm corresponding to mesoporous materials with an important contribution of adsorption in micropores. The H1-type hysteresis loop in the desorption branch of the material Z8P-5.00 indicates the presence of mesopores homogeneous in shape and size.[28] Neither interparticular adsorption nor hysteresis have been observed for the ZIF-8 NP, matching the microporous structure of this material. Therefore, the mesopores found in the sample Z8P-5.00 must be the interparticular volume between regular-in-size agglomerated nanocrystals, since the crystal phase is the same in both materials (Figures 1 and S1f; Supporting Information). The resulting high homogeneity in size and shape of mesopores could be a consequence of the interaction between chromophore molecules attached to the external surface of crystals, presumably acting as regular spacing agents between neighboring nanoparticles.

A lower amount of adsorbed N_2 at low P/P_0 indicates a lower porosity for Z8P-5.00. Table 2 compares the values of Brunauer−Emmett−Teller (BET) areas and micropore volumes, corroborating this reduction in porosity. Also, the

DOI: 10.1021/acsomega.9b01051
ACS Omega 2019, 4, 17090−17097

Table 2. Textural Properties and Densities of the ZIF-8 NP and Z8P-5.00

material	S_{BET} (m^2/g)	P/P_0 range for BET	$V_{\mu pore}$ (cm^3/g)	pore width (Å)	ρ_{sk} (g/cm^3)	ρ_{cr} (g/cm^3)	void volume (%)
ZIF-8 NP	1190 ± 20	0.008−0.03	0.52	0.88	1.45 ±0.02	0.83 ±0.02	63
Z8P-5.00	883 ± 10	0.008−0.05	0.36	0.74	1.40 ±0.02	0.93 ±0.02	39

apparent density was measured by He expansion, showing a slightly lower value for the material Z8P-5.00. Considering the micropore volume and not the total pore volume for the calculation, the resulting crystals after inclusion of the chromophore moiety have a higher density and a lower void volume. A larger mean pore size can be seen for the ZIF-8 NP when compared to that of Z8P-5.00 (Figure S5a in the Supporting Information and Table 2). The estimated values reasonably agree with the reported data (cavities of 1.2 nm of diameter connected by windows of 0.36 nm).[11] These differences in the pore size distribution (PSD) and the reduction in the void volume indicate the presence of some 1-aminopyrene molecules partially occupying the cavities of Z8P-5.00. Moreover, two pressure-adsorption steps can be seen on the N_2 adsorption isotherm for the ZIF-8 NP at values lower than 0.05 for P/P_0 that do not show for Z8P-5.00 (Figure 3). This behavior has been related to the rotation of the imidazole molecules in the window of the cage of the ZIF-8 structure,[29] and its absence in the modified material could be a consequence of the covalent inclusion of 1-aminopyrene molecules in the modified ZIF-8 structure. We believe the obtained data are conclusive to prove that the included aminopyrene functionality is not only on the external surface of the Z8P-5.00 nanocrystals but also inside of the pore cavities.

Spectrometric Characteristics of Z8P MOFs. The main principle used here to detect and quantify the presence of PAEs is fluorescence quenching, which is a well-established methodology.[30] In this particular system, the $\pi-\pi$ stacking interactions between the chromophore (pyrene covalently bound to the modified ZIF structure) and the aromatic analyte (PAEs) were supposed to be responsible for fluorescence relaxation leading to quenching.[20,31] The fluorescence quenching response of the system was studied focusing first on the dependency of the fluorescence for Z8P-5.00 in relation to its concentration (referring by concentration for Z8P MOFs as the mass of modified ZIF in "g" dispersed on a volume of methanol in "mL"). In Figure 4, the intensity increases as the concentration increases to 0.4 g·L^{-1}, then reaching a plateau.

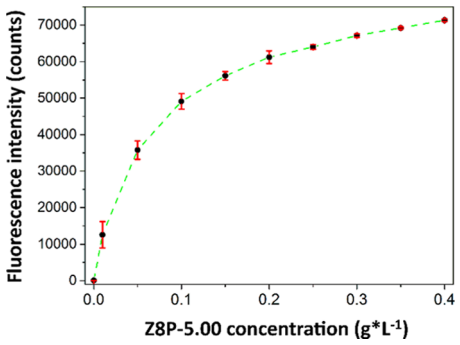

Figure 4. Fluorescence emission for Z8P-5.00 at different concentrations (from 0.00 to 0.4 g·L^{-1}). The intensity was taken from the emission maximum at 433 nm. The excitation wavelength was 277 nm. Each point was measured three times and the average results were plotted.

Since a modified ZIF concentration of 0.2 g·L^{-1} showed the beginning of the plateau, this is the range of concentrations for the modified ZIF that was chosen for the rest of the experiments.

Sensing with Z8P MOFs: Quantification of Four Different PAEs. The quenching of the fluorescence as a function of the concentration of PAEs was studied. Three Z8P-5.00 concentrations were chosen (0.20, 0.15, and 0.10 g·L^{-1}) and applied in the sensing of DMP in a concentration range from 0.00 to 2.00 g·L^{-1}. At low PAE concentrations, the quenching is not very pronounced. However, with increasing concentrations, saturation for the quenching is reached (Figure S4a, Supporting Information). Interestingly, in the chosen concentration range, a dependency on the Z8P-5.00 concentration could not be found. The effect of quenching is independent of the concentration for the sensing element within the concentration that was investigated (Supporting Information, Figure S4a).

When the fluorescence is tested in relation to the PAE concentration, a direct dependency between the loss in fluorescence emission intensity and the increase in the concentration of the analyte is observed (Figure 5). This is

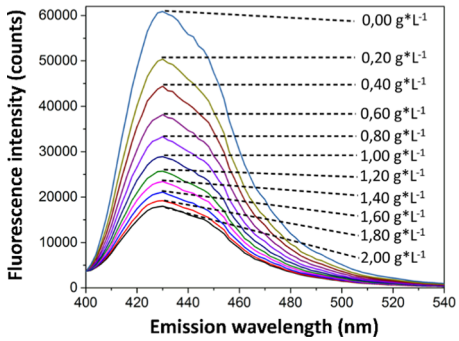

Figure 5. Fluorescence quenching measured with a fixed concentration of Z8P-5.00 (0.2 g·L^{-1}) is suspended in different solutions with varying concentrations of DMP (from 0.00, highest intensity curve, to 0.1 g·L^{-1}, lowest intensity curve). The excitation wavelength was 277 nm.

due to the quenching in fluorescence generated when the PAEs are near the covalently bound pyrene cores. Focusing on 0.20 g·L^{-1} for Z8P-5.00 and taking the intensity at the emission maximum at 430 nm for each concentration, a calibration curve was generated. The relation between fluorescence intensity and concentration for DMP proved to be nonlinear (Supporting Information, Figure S4b,c). Therefore, we applied the Stern−Volmer equation (eq 1) for collisional fluorescence quenching[23] to establish a functional relationship

$$\frac{F_0}{F_Q} = 1 + K_D \times Q \quad (1)$$

where F_0 is the fluorescence intensity for Z8P-5.00 with no quencher in the solution, F_Q is the fluorescence intensity for Z8P-5.00 in the presence of "Q" g·L^{-1} of DMP in solution, and K_D is the Stern−Volmer quenching constant for the system.

DOI: 10.1021/acsomega.9b01051
ACS Omega 2019, 4, 17090−17097

We assumed collisional quenching to be predominant over static quenching because the interaction between the fluorophore on Z8P-5.00 and the analyte is a soft and reversible $\pi-\pi$ stacking.

From the shape of the fitting (Supporting Information, Figure S4b), we can see that the assumption that there is only contribution from collisional quenching is wrong. It must be considered that there is also static quenching during the sensing process. Considering that it is highly unlikely that both the covalently bound aminopyrene and the analytes (phthalates molecules) can both fit at the same time inside the pore of the modified ZIF-8 and interact via $\pi-\pi$ interaction and given the relative sizes of the molecules and the pore size of ZIF-8, it should be assumed that the sensing takes place on the surface of the nanoparticle, with a very small contribution by the inside of the particle, generating a small static contribution to the quenching of the fluorescence.

With both static and dynamic quenching, a modified version of the Stern–Volmer equation that includes both contributions can be chosen

$$\frac{F_0}{F_Q} = (1 + K_D \times Q)(1 + K_S \times Q) \quad (2)$$

$$\frac{F_0}{F_Q} = 1 + (K_S + K_D) \times Q + K_S \times K_D \times Q^2 \quad (3)$$

where K_S is the association constant of the fluorophore–quencher complex. Applying this model, a very good fitting of the data is obtained (Figure 6). The resulting calibration curve

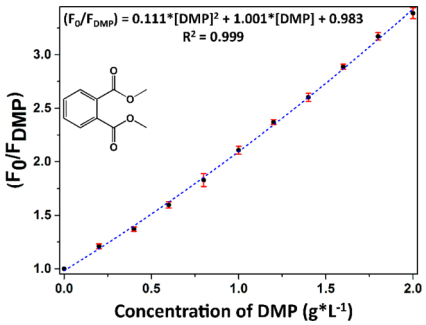

Figure 6. Modified Stern–Volmer fitting for the fluorescence quenching of Z8P-5.00 at different DMP concentrations (from 0.00 to 2.00 g·L^{-1}). The excitation wavelength was 277 nm, and the emission maximum was recorded at 430 nm. Each point was measured three times.

can be used to determine the concentration of all PAEs in the samples. The curve for the other PAEs (DBP, BBP, and DEHP) can be found in the Supporting Information, Figure S4d–f. The behavior of all chosen PAEs is very similar for DMP, DBP, and BBP, implying that there is no significant difference in the quenching process. DEHP shows a significant deviation from the rest. However, it seems possible to determine the sum of the concentration of a mixture of all of these species in a sample with high reliability.

We also calculated the limits of detection (LODs) from the obtained data.[32] The LODs range from 0.013 to 0.039 g·L^{-1} (Supporting Information, Figure S4f). For comparison, the most common methodology for the detection of phthalates to date is gas chromatography, and the reported LODs[33] are in the range of 0.006–0.17 μg·L^{-1}. The presented methodology clearly cannot compete with chromatography as a quantification method for very low concentrations, but this is not the objective of this application. Instead, we propose it as a complementary methodology for frequent surveys and/or in situ quantification and as the first step for a cheap and easy-to-use alternative, potentially a process analytical sensor in phthalates' production.

CONCLUSIONS

Modified ZIF-8 fluorescent MOF nanoparticles were synthesized with a distribution ranging between 20 and 50 nm in diameter, with the synthesis showing a high reproducibility. We have shown an easy synthetic route and how to tune the fluorescence of the modified ZIF, by varying the amount of pyrene derivative added to the ZIF-8 structure. HPLC quantification of the modified ZIF constituents was able to prove that the initial stoichiometry of the synthesis proportion influences the final composition of the modified ZIF.

Fluorescence studies resulted in concentration/signal relationships for all of the chosen analytes, four phthalate esters. A modified Stern–Volmer model fitted perfectly the calibration relationship. We proved that this modified ZIF-8 is a good first step towards the development of a cheap and easy-to-use device to detect the presence of PAEs. The selectivity of the system relies mostly on the sample type and pretreatment since small aromatic molecules will most likely interfere with the quenching. However, if the pretreatment of the sample is adequate, this modified ZIF could be part of a continuous and cost-effective surveillance system, applicable to wastewaters from industrial production, for example.

EXPERIMENTAL SECTION

Reagents. The PAEs were obtained from Sigma-Aldrich: dimethylphthalate ≥99% (DMP), dibutylphthalate 99% (DBP), benzylbutylphthalate 98% (BBP), and diethylhexylphthalate ≥99.5% (DEHP).

Zinc nitrate hexahydrate ≥99% was bought from Roth; 2-methylimidazol 99% (2-MeImi) was from Acros Organics; 1-

Table 3. Amounts for Each of the Reagents for the Synthesis of Each of the Variants for Z8P MOFs

	Z8P-0.25	Z8P-0.50	Z8P-0.75	Z8P-1.00	Z8P-2.50	Z8P-5.00
2-imidazolecarboxaldehyde	0.72 mg	1.44 mg	2.16 mg	2.88 mg	7.21 mg	14.41 mg
	0.0075 mmol	0.0150 mmol	0.023 mmol	0.030 mmol	0.075 mmol	0.150 mmol
1-aminopyrene	1.630 mg	3.259 mg	4.889 mg	6.518 mg	16.295 mg	32.591 mg
	0.0075 mmol	0.0150 mmol	0.023 mmol	0.030 mmol	0.075 mmol	0.150 mmol
2-methylimidazol	61.267 mg	60.959 mg	60.651 mg	60.344 mg	58.496 mg	55.418 mg
	0.750 mmol	0.7425 mmol	0.7387 mmol	0.735 mmol	0.7125 mmol	0.675 mmol
1-methylimidazol	61.267 mg	60.959 mg	60.651 mg	60.344 mg	58.496 mg	55.418 mg
	0.750 mmol	0.7425 mmol	0.7387 mmol	0.735 mmol	0.7125 mmol	0.675 mmol

DOI: 10.1021/acsomega.9b01051
ACS Omega 2019, 4, 17090–17097

methylimidazol 99% (1-MeImi) was obtained from Fluorochem; *n*-butylamine 99.5%, 1-aminopyrene 97% (1-AmiPyr), and 2-imidazolecarboxaldehyde 97% (2-ImiCarb) were purchased from Sigma-Aldrich.

Preparation of the 1-aminopyrene-functionalized ZIF-8 nanoparticles (Z8P-0.25 to Z8P-5.00). Samples with different ratios of 2-imidazolcarboxaldehyde and 1-aminopyrene (see Table 3) were dissolved in 7.5 mL of methanol in a sealed glass flask, and then heated to 90 °C for 30 min. Afterward, 146 μL of *n*-butylamine (2.700 mmol) was added to the mix and stirred for 10 min. After cooling to ambient temperature, a varying amount of 2-methylimidazole and 1-methylimidazole was added to the mix. Finally, a methanolic solution (12 mL) with 112 mg (0.377 mmol) of $Zn(NO_3)_2$ and $6H_2O$ was added to the mix. Almost immediately, a yellow precipitate appeared suspended in the solution. The mixture was left undisturbed for 8 h. The solid was extracted via centrifugation, washed three times with methanol, and dried at room temperature at ambient pressure. The nomenclature used here for each of the modified ZIFs is in reference to the molar percentage of the 1-aminopyrene for their synthesis.

Preparation of the Nanoparticulate ZIF-8. A total of 1.5 mmol (122.534 mg) of 2-methylimidazole was dissolved in 7.5 mL methanol in a glass flask, together with 146 μL of *n*-butylamine (2.700 mmol), and the mix was stirred for 10 min. A methanolic solution (12 mL) with 112 mg (0.377 mmol) of $Zn(NO_3)_2$ and $6H_2O$ was added to the first mix. Almost immediately, a white precipitate appeared suspended in the solution. The mixture was left undisturbed for 8 h. The solid was extracted via centrifugation, washed three times with methanol, and dried at room temperature at ambient pressure.

Methods. *Powder X-ray Diffractometry.* Powder X-ray diffractometry patterns were collected with Cu Kα radiation (λ = 1.50406 nm) on a D8 Advanced diffractometer (Bruker AXS, Germany) equipped with a Lynxeye detector. Samples were measured in reflection geometry in a 2θ range from 4 to 60° with a step size of 0.009°.

Fluorescence Measurements. Fluorescence spectra were obtained on an all-in-one microplate reader Synergy H1 with dispenser (BioTek). The software used was Gen5. The spectra were acquired from 380 to 600 nm, with a step of 2 nm, the measurement time of 10 ms, and the delay between measurements of 100 ms. The samples were handled in a polypropylene 96-well black plate from Greiner Bio-One.

HPLC–UV. The HPLC measurements were performed on a SECurity GPC System (PSS GmbH) with a SeQuant ZIC-HILIC 3.5 μm, 100 Å sorbent, Peek 150 × 4.6 mm^2 metal-free HPLC column (di2chrom/Merck). The autosampler and column were operated at 35 °C. UV absorption at a wavelength of 230 nm was recorded. The mobile phase was a mixture of 65% acetonitrile and 35% H_2O, containing 0.1% trifluoroacetic acid. The injected volume was 5 μL. The flow rate was 1 $mL{\cdot}min^{-1}$. The samples were dissolved in the mobile phase mixture. HPLC/MS grade solvents (Honeywell, Riedel-dee-Haën) were used.

Mass Spectrometry Measurements. The mass spectrometric measurements were performed on a Q-TOF Ultima ESI-TOF mass spectrometer (Micromass), operating in positive ion mode at a capillary voltage of 2–3 kV, a cone voltage of 35 V, and collision energy of 5 eV. The source temperature was 120 °C and the desolvation temperature was 150 °C.

TEM Measurements. TEM measurements were performed on a ThermoFisher Scientific Talos F200S 200 kV scanning/transmission electron microscope, using a copper ultra-thin C film on Lacey Carbon support film with a 400 mesh.

N_2 Adsorption–Desorption Experiments at −196 °C. N_2 adsorption–desorption isotherms were measured at 77 K on a volumetric ASAP 2020 device (Micromeritics) in the range of relative pressures P/P_0 from 10^{-7} to 0.996. For analysis, 0.3 g of each material was loaded in the analysis probe, followed by thermal activation at 160 °C for 18 h under a minimum vacuum pressure below 10^{-6} mbar. The warm and cold free spaces were estimated after He expansion after the N_2 experiment. BET area was calculated by following Rouquerol and Llewellyn's rule for the selection of the optimal BET range.[27] Pore size distribution (PSD) and micropore volume were estimated by nonlocal density functional theory (NL-DFT) by Microactive 5.01 software. The used model kernel was that for cylindrical pore geometry "N_2 Tarazona NL-DFT, Esf = 30.0 K", according to the best fitting of data (see Figure S5b,c in the Supporting Information) and the comparison of results with the reported crystallographic information for the ZIF-8 structure.[11] The micropore volume was assumed as the corresponding cumulative pore volume for pore sizes of 22 Å.

Sample Density. Apparent sample density was measured by comparing the free-space measurement of the occupied analysis cell with the sample with the empty analysis cell in a Sieverts-like apparatus (Micromeritics HPVA II). It was measured at the beginning of the analysis by He expansion at ambient temperature in 40 repetitions with intermediate evacuation for 20 min. Gas density was calculated from *P* and *T* values by using the modified Benedict–Webb–Rubin equation of state for Helium of McCarty and Arp, as recommended by National Institute of Standards and Technology.[34] The room temperature where the device is located is stable within ±1 °C, and the manifold temperature is constant at 32–33 °C. The value of the free space of the empty analysis cell was averaged from 100 measurements, and the accuracy and linearity of the free volume measurements for solid samples were checked by calibration with different amounts of a nonporous SiO_2 reference material CRM BAM-PM-101, whose density was previously certified by BAM. According to this calibration, each measurement of the sample volume herein has an accuracy of 96–98% for an occupancy of the analysis cell free volume from 5 to 70%, respectively. In a typical experiment, 0.5–0.7 g of fresh material were loaded in the analysis cell, whose empty weight was considered as an average value of 100 measurements. Before analysis, samples were degassed at 160 °C for 18 h at dynamic high vacuum (pressure lower than 10^{-6} mbar). Crystal density (ρ_{cr}) and the void volume fraction were calculated from the apparent sample density (ρ_{sk}) and the micropore volume ($v_{\mu pore}$) by using eqs 4 and 5, respectively.

$$\rho_{cr} = \frac{\rho_{sk}}{\frac{v_{\mu pore}}{\rho_{sk}} + 1} \tag{4}$$

$$\text{void volume} = \frac{v_{\mu pore}}{\rho_{cr}}. \tag{5}$$

■ ASSOCIATED CONTENT

Supporting Information

The Supporting Information is available free of charge on the ACS Publications website at DOI: 10.1021/acsomega.9b01051.

DOI: 10.1021/acsomega.9b01051
ACS Omega 2019, 4, 17090–17097

Structural characterization of the modified ZIFs via PXRD; particle size distribution characterization via electron microscopy; composition determination of the modified ZIFs via HPLC; photophysical characterization of the modified ZIFs; pore size distribution studies for the obtained ZIFs (PDF)

AUTHOR INFORMATION

Corresponding Author

*E-mail: franziska.emmerling@bam.de.

ORCID

Jana Falkenhagen: 0000-0001-7772-606X
Rudolf J. Schneider: 0000-0003-2228-1248
Franziska Emmerling: 0000-0001-8528-0301

Notes

The authors declare no competing financial interest.

ACKNOWLEDGMENTS

A.C.-A. acknowledges the School of Analytical Sciences Adlershof (SALSA) for personal financial support.

REFERENCES

(1) Albert, O.; Jegou, B. A critical assessment of the endocrine susceptibility of the human testis to phthalates from fetal life to adulthood. *Hum. Reprod. Update* **2014**, *20*, 231−249.

(2) Latini, G. Monitoring phthalate exposure in humans. *Clin. Chim. Acta* **2005**, *361*, 20−29.

(3) Heudorf, U.; Mersch-Sundermann, V.; Angerer, J. Phthalates: toxicology and exposure. *Int. J. Hyg. Environ. Health* **2007**, *210*, 623−634.

(4) Net, S.; Delmont, A.; Sempere, R.; Paluselli, A.; Ouddane, B. Reliable quantification of phthalates in environmental matrices (air, water, sludge, sediment and soil): a review. *Sci. Total Environ.* **2015**, *515*−*516*, 162−180.

(5) Xu, F.; Wang, W. J.; Jiang, H. Y.; Wang, Z. P.; Wang, Z. H.; Guo, P.; Sun, S. Y.; Ding, S. Y. Indirect Competitive Enzyme-Linked Immunosorbent Assay for the Detection of Dibutyl Phthalate in White Wine, Compared With GC-MS. *Food Anal. Methods* **2014**, *7*, 1619−1626.

(6) Zhang, M. C.; Wang, Q. E.; Zhuang, H. S. A novel competitive fluorescence immunoassay for the determination of dibutyl phthalate. *Anal. Bioanal. Chem.* **2006**, *386*, 1401−1406.

(7) Wei, C.; Ding, S.; You, H.; Zhang, Y.; Wang, Y.; Yang, X.; Yuan, J. An immunoassay for dibutyl phthalate based on direct hapten linkage to the polystyrene surface of microtiter plates. *PLoS One* **2011**, *6*, No. e29196.

(8) Sun, R. Y.; Zhuang, H. S. An indirect competitive biotin-streptavidin enzyme-linked immunosorbent assay for the determination of dimethyl phthalate (DMP) in milk and milk products. *J. Environ. Sci. Health, Part B* **2015**, *50*, 275−284.

(9) Baldofski, S.; Canitz, C. J.; Garbe, L. A.; Schneider, R. J. Studies on the development of antibodies for the highly hydrophobic plasticizers DINCH and DEHT. *Anal. Biochem.* **2018**, *543*, 90−96.

(10) Hayashi, H.; Cote, A. P.; Furukawa, H.; O'Keeffe, M.; Yaghi, O. M. Zeolite A imidazolate frameworks. *Nat. Mater.* **2007**, *6*, 501−506.

(11) Park, K. S.; Ni, Z.; Cote, A. P.; Choi, J. Y.; Huang, R.; Uribe-Romo, F. J.; Chae, H. K.; O'Keeffe, M.; Yaghi, O. M. Exceptional chemical and thermal stability of zeolitic imidazolate frameworks. *Proc. Natl. Acad. Sci. U.S.A.* **2006**, *103*, 10186−10191.

(12) Beyer, S.; Prinz, C.; Schürmann, R.; Feldmann, I.; Zimathies, A.; Blocki, A. M.; Bald, I.; Schneider, R. J.; Emmerling, F. Ultra-Sonication of ZIF-67 Crystals Results in ZIF-67 Nano-Flakes. *ChemistrySelect* **2016**, *1*, 5905−5908.

(13) Kulow, A.; Witte, S.; Beyer, S.; Buzanich, A. G.; Radtke, M.; Reinholz, U.; Riesemeier, H.; Streli, C. A new experimental setup for time- and laterally-resolved X-ray absorption fine structure spectroscopy in a 'single shot'. *J. Anal. At. Spectrom.* **2019**, *34*, 239−246.

(14) Kaneti, Y. V.; Dutta, S.; Hossain, M. S. A.; Shiddiky, M. J. A.; Tung, K. L.; Shieh, F. K.; Tsung, C. K.; Wu, K. C.; Yamauchi, Y. Strategies for Improving the Functionality of Zeolitic Imidazolate Frameworks: Tailoring Nanoarchitectures for Functional Applications. *Adv. Mater.* **2017**, *29*, No. 1700213.

(15) Yan, B. Lanthanide-Functionalized Metal-Organic Framework Hybrid Systems To Create Multiple Luminescent Centers for Chemical Sensing. *Acc. Chem. Res.* **2017**, *50*, 2789−2798.

(16) Jia, H. X.; Yao, Y. C.; Zhao, J. T.; Gao, Y. Y.; Luo, Z. L.; Du, P. W. A novel two-dimensional nickel phthalocyanine-based metal-organic framework for highly efficient water oxidation catalysis. *J. Mater. Chem. A* **2018**, *6*, 1188−1195.

(17) Maya, F.; Cabello, C. P.; Clavijo, S.; Estela, J. M.; Cerda, V.; Palomino, G. T. Zeolitic imidazolate framework dispersions for the fast and highly efficient extraction of organic micropollutants. *RSC Adv.* **2015**, *5*, 28203−28210.

(18) Ortiz, A. U.; Freitas, A. P.; Boutin, A.; Fuchs, A. H.; Coudert, F.-X. What makes zeolitic imidazolate frameworks hydrophobic or hydrophilic? The impact of geometry and functionalization on water adsorption. *Phys. Chem. Chem. Phys.* **2014**, *16*, 9940−9949.

(19) Seo, P. W.; Bhadra, B. N.; Ahmed, I.; Khan, N. A.; Jhung, S. H. Adsorptive Removal of Pharmaceuticals and Personal Care Products from Water with Functionalized Metal-organic Frameworks: Remarkable Adsorbents with Hydrogen-bonding Abilities. *Sci. Rep.* **2016**, *6*, No. 34462.

(20) Rochat, S.; Steinmann, S. N.; Corminboeuf, C.; Severin, K. Fluorescence sensing of caffeine in water with polysulfonated pyrenes. *Chem. Commun.* **2011**, *47*, 10584−10586.

(21) Cravillon, J.; Nayuk, R.; Springer, S.; Feldhoff, A.; Huber, K.; Wiebcke, M. Controlling Zeolitic Imidazolate Framework Nano- and Microcrystal Formation: Insight into Crystal Growth by Time-Resolved In Situ Static Light Scattering. *Chem. Mater.* **2011**, *23*, 2130−2141.

(22) Morris, W.; Doonan, C. J.; Furukawa, H.; Banerjee, R.; Yaghi, O. M. Crystals as Molecules: Postsynthesis Covalent Functionalization of Zeolitic Imidazolate Frameworks. *J. Am. Chem. Soc.* **2008**, *130*, 12626−12627.

(23) Albrecht, C. Principles of fluorescence spectroscopy. *Anal. Bioanal. Chem.* **2008**, *390*, 1223−1224.

(24) Beyer, S.; Schurmann, R.; Feldmann, I.; Blocki, A.; Bald, I.; Schneider, R. J.; Emmerling, F. Maintaining Stable Zeolitic Imidazolate Framework (ZIF) Templates during Polyelectrolyte Multilayer Coating. *Colloid Interface Sci. Commun.* **2018**, *22*, 14−17.

(25) Widmer, R. N.; Lampronti, G. I.; Anzellini, S.; Gaillac, R.; Farsang, S.; Zhou, C.; Belenguer, A. M.; Wilson, C. W.; Palmer, H.; Kleppe, A. K.; Wharmby, M. T.; Yu, X.; Cohen, S. M.; Telfer, S. G.; Redfern, S. A. T.; Coudert, F.-X.; MacLeod, S. G.; Bennett, T. D. Pressure promoted low-temperature melting of metal−organic frameworks. *Nat. Mater.* **2019**, *18*, 370−376.

(26) Layer, R. W. The Chemistry of Imines. *Chem. Rev.* **1963**, *63*, 489−510.

(27) Thommes, M.; Kaneko, K.; Neimark, A. V.; Olivier, J. P.; Rodriguez-Reinoso, F.; Rouquerol, J.; Sing, K. S. W. Physisorption of gases, with special reference to the evaluation of surface area and pore size distribution (IUPAC Technical Report). *Pure Appl. Chem.* **2015**, *87*, 1051−1069.

(28) Horikawa, T.; Do, D. D.; Nicholson, D. Capillary condensation of adsorbates in porous materials. *Adv. Colloid Interface Sci.* **2011**, *169*, 40−58.

(29) Fairen-Jimenez, D.; Moggach, S. A.; Wharmby, M. T.; Wright, P. A.; Parsons, S.; Duren, T. Opening the gate: framework flexibility in ZIF-8 explored by experiments and simulations. *J. Am. Chem. Soc.* **2011**, *133*, 8900−8902.

(30) Rehm, D.; Weller, A. Kinetics of fluorescence quenching by electron and H-atom transfer. *Isr. J. Chem.* **1970**, *8*, 259−271.

(31) Kowalczyk, T.; Lin, Z.; Van Voorhis, T. Fluorescence quenching by photoinduced electron transfer in the Zn^{2+} sensor

DOI: 10.1021/acsomega.9b01051
ACS Omega 2019, 4, 17090−17097

zinpyr-1: a computational investigation. *J. Phys. Chem. A* **2010**, *114*, 10427−10434.
(32) Armbruster, D. A.; Pry, T. Limit of blank, limit of detection and limit of quantitation. *Clin. Biochem. Rev.* **2008**, *29*, S49−S52.
(33) Peñalver, A.; Pocurull, E.; Borrull, F.; Marce, R. M. Determination of phthalate esters in water samples by solid-phase microextraction and gas chromatography with mass spectrometric detection. *J. Chromatogr. A* **2000**, *872*, 191−201.
(34) Arp, V. D. State equation of liquid helium-4 from 0.8 to 2.5 K. *J. Low Temp. Phys.* **1990**, *79*, 93−114.

DOI: 10.1021/acsomega.9b01051
ACS Omega 2019, 4, 17090−17097